JBMR Plus, 2025, **9**, ziaf067
https://doi.org/10.1093/jbmrpl/ziaf067
Advance access publication: April 16, 2025
Research Article

Expression of the aryl hydrocarbon receptor in Osterix-lineage cells regulates adult skeletal homeostasis in a compartment-specific manner

Jennifer Dorn[1], Dima W. Alhamad[1], Husam Bensreti[1], Christopher L. Yearwood[1], Tate J. Allen[1], Michaela Cushing[1], Joseph C. Shaver[1], Colby Gross[1], William C. Whichard[1], Caihong Dai[1], Kanglun Yu[1], Roger Zhong[2], Marion A. Cooley[3], Maribeth H. Johnson[2], Wendy B. Bollag[4,5], Sadanand Fulzele[6], Carlos M. Isales[2,6], Mark W. Hamrick[1], William D. Hill[7], Meghan E. McGee-Lawrence[1,*]

[1]Department of Cellular Biology and Anatomy, Medical College of Georgia Augusta University, Augusta, GA 30912, United States
[2]Department of Neuroscience and Regenerative Medicine, Medical College of Georgia, Augusta University, Augusta, GA 30912, United States
[3]Department of Oral Biology and Diagnostic Sciences, Dental College of Georgia, Augusta University, Augusta GA 30912, United States
[4]Department of Physiology, Medical College of Georgia Augusta University, Augusta, GA 30912, United States
[5]Charlie Norwood VA Medical Center, Augusta, GA 30912, United States
[6]Department of Medicine, Medical College of Georgia Augusta University, Augusta, GA 30912, United States
[7]Department of Pathology, Medical University of South Carolina, Charleston, SC 29403, United States

*Corresponding author:Meghan E. McGee-Lawrence, Department of Cellular Biology and Anatomy, Medical College of Georgia Augusta University, 1120 15th Street, CB1101, Augusta, GA 30912, United States (mmcgeelawrence@augusta.edu).

Abstract

Kynurenine (KYN), a tryptophan metabolite that increases with age, impairs osteoblast function. The aryl hydrocarbon receptor (AhR) has been proposed to mediate KYN's actions in bone. To test whether deletion of AhR in osteoblasts is beneficial for bone, we established an adult-onset AhR conditional knockout (CKO) model using Osx-Cre and examined the effects of AhR CKO at 4.5 and 6 mo of age (representing ~6 and 12 wk of CKO). While BMSC-derived osteoblasts from WT mice demonstrated reduced matrix formation from KYN treatment, AhR CKO osteoblasts were unaffected by KYN. Kynurenine's harmful effects were most pronounced in the middle of an osteoblastic differentiation time course, and these effects could be rescued via the AhR antagonist BAY2416964. In vivo, AhR deletion in Osx-expressing cells promoted sex- and compartment-specific skeletal phenotypes. Trabecular bone was increased in the distal femur of male and female AhR CKO mice at both 4.5 and 6 mo of age, potentially driven by a net decrease in the ratio of trabecular osteoclasts to osteoblasts despite a reduction in mineral apposition rate at 6 mo of age. In contrast, cortical bone phenotypes induced by AhR deletion depended on age and sex. In males, cortical bone volume fraction (Ct.BV/TV) was elevated in AhR CKO mice vs WT littermates at 4.5 mo of age, but differences resolved by 6 mo of age. In contrast, cortical bone was reduced in female AhR CKO as compared to WT littermates at 6 mo of age. These results underscore the complexity of AhR signaling in skeletal biology that must be considered while exploring AhR as a therapeutic target for conditions like osteoporosis and musculoskeletal frailty. Future studies will be needed to test the effects of osteoblastic AhR deletion at advanced ages, when the endogenous AhR ligand KYN is elevated in the circulation and skeletal niche.

Keywords: bone, aging, osteoblast, kynurenine, AhR

Lay Summary

Kynurenine (KYN) increases with age and causes bone loss. Osteoblasts make less bone when treated with KYN, but inhibiting or genetically deleting the aryl hydrocarbon receptor (AhR) in cell cultures prevented this outcome. When AhR was deleted from osteoblasts in mice, both male and female AhR-deficient mice developed high spongy bone mass, whereas male AhR-deficient mice developed a transient increase incompact bone, and female AhR-deficient mice showed an eventual decrease in compact bone. These studies were conducted on young mice when KYN levels are low; targeting AhR may show greater benefits in older animals when KYN levels are higher.

Received: January 10, 2025. **Revised:** March 24, 2025. **Accepted:** April 2, 2025

Graphical Abstract

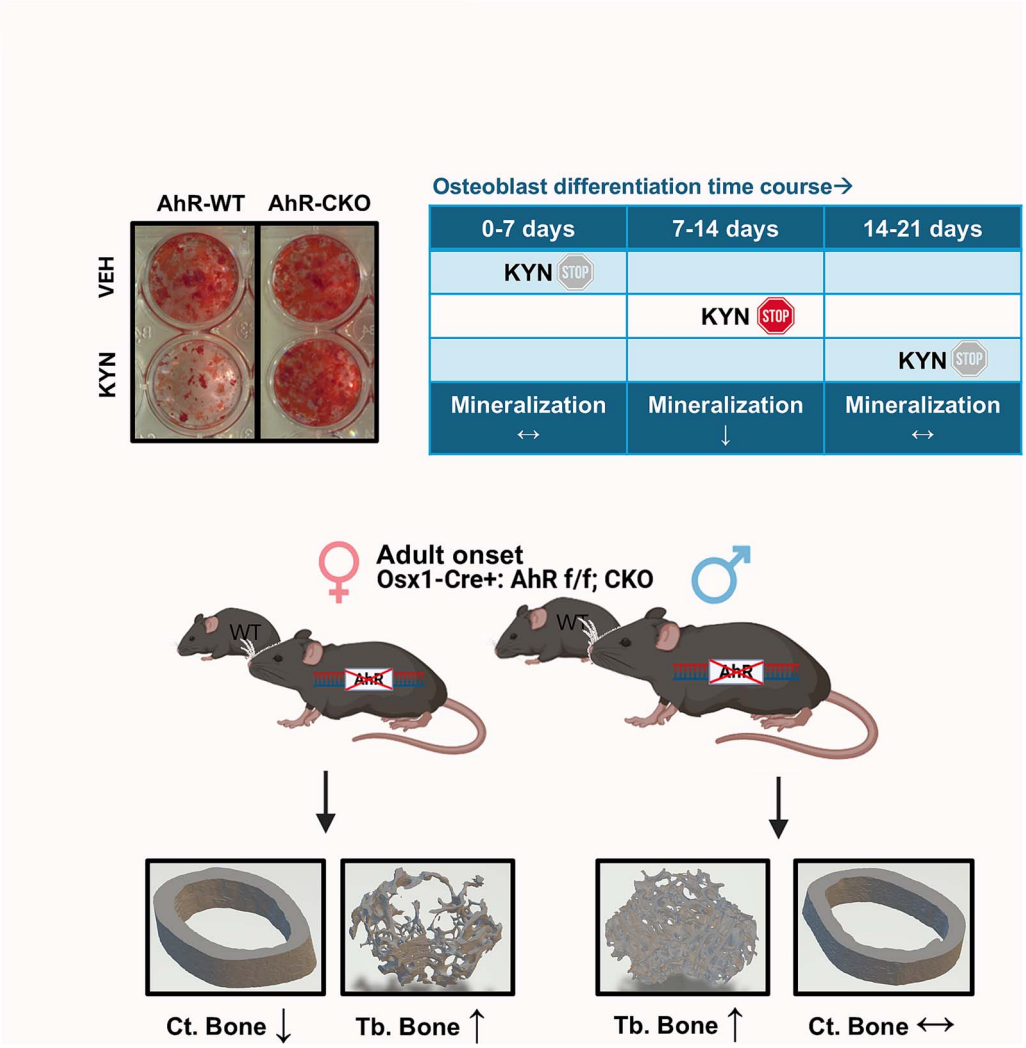

Introduction

Osteoporosis is a skeletal disease resulting from an imbalance between bone matrix formation by osteoblasts and bone resorption by osteoclasts. Although many environmental factors can contribute to the pathogenesis and severity of osteoporosis, this condition can be exacerbated by a low-protein diet typically seen with an age-dependent loss of nutrient sensing.[1] The negative effects of a low protein diet on bone can be at least partly ameliorated via supplementation with aromatic amino acids such as tryptophan.[1] Tryptophan is anabolic for osteoblasts[2] but this benefit is lost when it is oxidized by enzymes including indoleamine 2,3-dioxygenase and tryptophan 2,3-dioxygenase into downstream metabolites in the kynurenine (KYN) pathway.[3] The activity of these tryptophan-metabolizing enzymes increases with age in response to increased inflammation.[3–5] The first metabolite of this pathway is KYN, the concentration of which increases in circulation with age in both mice and humans.[6–8] Kynurenine levels are highest in human patients classified as frail (defined as having low bone and muscle mass that predisposes patients to fracture) as compared to healthier, age-matched controls.[9] Consistent with this observation, local KYN levels in bone marrow are significantly higher in patients who have suffered hip fractures as compared to nonfractured controls.[9]

While several studies report correlations between elevated KYN levels and poor musculoskeletal health, previous research also supports KYN as a causative factor for musculoskeletal frailty. Kynurenine treatment clearly stimulates bone resorption activity by osteoclasts,[10] but its harmful effects on mesenchymal lineage progenitor populations and on mature osteoblasts also contribute to overall declines in bone mass following KYN administration. Mechanistically, KYN induced oxidative stress and senescence in bone marrow stromal cell (BMSC) osteoprogenitor populations,[11,12] impaired osteogenic differentiation of BMSC, and blunted mineralized matrix production by BMSC-derived osteoblasts.[6] Dietary administration of KYN to 12-mo-old male C57BL6/J mice led to decreased bone mass caused in part by decreased bone formation activity as compared to vehicle-treated mice.[6] These dietary effects of KYN were recapitulated by administering KYN via i.p. injection, where 20 mg/kg daily KYN administration to male CD-1 mice suppressed bone formation activity in vivo.[6] Consistent with in vitro data that support a direct, inhibitory effect of KYN on

osteoblastic function, adult female C57BL/6 mice treated with 10 mg/kg KYN for 4 wk showed a significant reduction in osteoblast number as compared to sex-matched vehicle-treated mice.[13,14] Dietary KYN treatment also promoted an increase in relative bone marrow adipose tissue (BMAT) abundance and bone marrow adipocyte numbers,[6] suggesting alterations to the bone marrow niche.

The molecular mediator of KYN-induced osteoblast dysfunction has not yet been conclusively identified. Kynurenine is an aromatic molecule that is transported into the cytoplasm via transporters such as Slc7a5 (LAT1) and Slc7a11.[15–17] It has been previously demonstrated that KYN is an endogenous ligand for the aryl hydrocarbon receptor (AhR),[18,19] and inhibitor-based studies have suggested that AhR may mediate the negative effects of KYN in mesenchymal progenitor cells.[11] The AhR can also bind a multitude of other exogenous and endogenous ligands including 2,3,7,8-tetrachlorodibenzo-p-dioxin (TCDD), polycyclic aromatic hydrocarbons, benzo(a)pyrene, 6-formylindolo[3,2-b]carbazole (FICZ), tryptamine, and carotenoids,[20] and AhR-mediated signaling induces diverse, ligand-specific effects across cell types. Upon ligand binding, AhR signaling has been reported to alter transcription, cell cycle regulation, and epigenetic mechanisms such as DNA methylation, posttranslational histone modification, chromatin remodeling, and microRNA signaling.[21,22] These and other AhR-mediated signaling events can promote physiological processes, such as inflammation, altered cell energetics, and immune regulation.[23] AhR mediates the toxic effects of TCDD, but also has been reported to drive detoxification,[22] and likewise has been reported to mediate both cell migration and cell adhesion.[22] Contradictory evidence is similarly reported in the literature surrounding AhR's effects on bone cells.[24] In osteoprogenitor cells, AhR has been reported to be both beneficial[25,26] as well as inhibitory,[27–29] and similar discrepancies exist in other cell populations such as osteoclasts[30–32] and chondrocytes.[26,33,34] One caveat is that the role of AhR in these previous studies has been ascertained largely via the use of pharmacological inhibitors against AhR and exogenous AhR ligands already known to act as toxicants. Pharmacological inhibitors can have off-target effects that may confound understanding of endogenous processes.[35] To date, genetic tools have not been applied to understand the role of AhR in mediating the functions of endogenous ligands, like tryptophan metabolites, in osteoblast linage cells. Accordingly, the goal of the current study was to determine the role of osteoprogenitor AhR in postnatal skeletal homeostasis and in mediating the downstream effects of KYN in this cell population.

Materials and methods

Animals

The research was conducted according to guidelines provided by the National Institutes of Health (NIH) and under protocols approved by the Augusta University Institutional Animal Care and Use Committee. All animals were group-housed in an accredited facility and maintained on a 12-hr light/dark cycle. Mice containing loxP sites surrounding exon 2 of the AhR (D-allele) gene and mice expressing Cre under control of the Osx promoter were obtained from The Jackson Laboratory (JAX #006203 and JAX# 006361, respectively) and crossed to generate AhR conditional knockout (CKO) (Osx1-Cre+: AhR f/f) and wildtype control (Osx-Cre-: AhR f/f; WT) littermates. Breeding pairs and subsequent progeny were maintained on a doxycycline-containing chow diet (Teklad #TD.120769; 625 mg/kg) until 12 wk of age to delay Cre expression until the rapid phase of skeletal growth has subsided, followed by a standard rodent diet (Teklad 2018, Envigo) to promote Cre expression as previously described.[36] An additional cohort of Cre + WT (ie, Osx1-Cre+: AhR+/+) and Cre − WT (Osx1-Cre-: AhR+/+) mice were maintained with identical dietary conditions (ie, doxycycline-containing chow until 12 wk of age followed by standard rodent diet thereafter) to test for the presence of any Cre-driven skeletal phenotypes in the absence of AhR deletion via micro-computed tomography. Mice were allowed food and water ad libitum unless otherwise stated for an experiment. Mice received an i.p. injection with 10 mg/kg calcein (Sigma #C0875) on days 8 and 1 prior to being euthanized via carbon dioxide inhalation.

Tissue specificity of Osx-Cre activity in adult-onset CKO model

Tissues collected from WT and AhR CKO mice at sacrifice, including bone, brain, heart, kidneys, and spleens were processed using a genomic DNA purification kit (Thermofisher GeneJET #FERK0722) to isolate genomic DNA which was then subjected to polymerase chain reactions (PCR) as described previously.[37,38] Primer sequences are listed in Table S1. To assess Cre-mediated DNA recombination, PCR products were visualized on a 2% agarose gel with ethidium bromide using a Bio-Rad ChemiDoc XRS+ imaging system.

BMSC isolation and primary cell culture

Primary BMSC were harvested from long bones by syringe flush of bone marrow using cell culture growth medium consisting of minimum essential medium (MEM)-α (Gibco #12561-072; Thermo Fisher Scientific) + 20% fetal bovine serum (FBS; Atlanta Biologicals #S11150H or Corning #35-010-CV) + 1% antibiotic-antimycotic (Gibco #15240-062) + 1% MEM nonessential amino acids (Gibco #11140-050). Osteogenic induction (to obtain primary BMSC-derived osteoblasts; BMSC-OB) began at seeding (day 0) in 12-well plates (Corning #0720082) at 4 million cells/well using cell culture growth medium supplemented with ascorbic acid (50 μg/mL; Sigma-Aldrich #A4544) and β-glycerophosphate (10 mM; Sigma-Aldrich #G9422) in the presence or absence of KYN (Millipore Sigma #K8625, 100 μM). The culture medium was changed every 3-4 d. To assess mineralized matrix formation, BMSC-OB cultures were maintained for 21 d in the indicated treatments and fixed with 10% neutral-buffered formalin for at least 1 hr, and then stained for 10 min with Alizarin Red S (Sigma-Aldrich #A5533). The stained area normalized to the total well area was quantified with Bioquant Osteo. Cultures were also stained with 0.5% Crystal Violet solution (Fisher #C581-25) to assess colony formation and cell density, where the Crystal Violet-stained area and total well area were quantified with Bioquant Osteo. Metrics of Alizarin Red and Crystal Violet staining were compared between groups, and Alizarin Red staining was also normalized to Crystal Violet staining to estimate the mineralized matrix on a per-cell basis as an additional endpoint.

Analysis of conditioned medium from BMSC-derived osteoblasts

Conditioned medium was collected from BMSC-OB cultures derived from 6-mo-old mice during day 7 and day 14 of differentiation. Protein levels of RANK ligand (RANKL), macrophage colony-stimulating factor (M-CSF), and osteoprotegerin (OPG) were detected in the conditioned medium with Biotechne panels utilizing Luminex-based technology (Biotechne Cat# LXSAMSM and #TNFRSF11B) according to manufacturer's instructions. In brief, samples and standards were added to a 96 well plate and incubated with magnetic bead-conjugated capture antibodies overnight at 4 °C on a plate shaker. After washing the plate using a Bio-Plex Pro Wash Station (BioRad Cat# 30034376), biotinylated detection antibodies were added to each well and the plate was incubated on a shaker (600 rpm) for 1 hr at room temperature. Finally, after washing, SA-PE was added and incubated for 30 min. Samples were acquired on Luminex FLEXMAP 3D instrument (Thermo Cat# APX1342). Standard curves and protein concentration were calculated using Quantist Luminex Data Analysis Software (Biotechne). Assay and data calculations were performed by the Georgia Cancer Center Immune Monitoring Shared Resource at Augusta University. Samples with analyte levels below the limit of detection were excluded from analysis.

Immortalized cell cultures

Immortalized osteoprogenitor MC3T3 (subclone 4) cells were used to determine the impact of AhR inhibition (via BAY2416964) on the production of osteoblastic matrix throughout various stages of osteoblast differentiation. MC3T3 cells were expanded in growth media consisting of ascorbic acid-free α MEM (Fisher #A1049001), 10% FBS (Corning #35-010-CV), and 1% Penicillin/Streptomycin (Corning #30002Cl). Cells were seeded in 12-well plates (Corning #0720082) at 35 000 cells per well in growth media supplemented with 10 mM beta glycerol phosphate (Santa Cruz #SC-220452) and 50 μg/mL ascorbic acid (Sigma, #A4544) to promote osteoblastic differentiation. Cells were maintained for 21 d in the indicated treatments including KYN (Millipore Sigma #K8625, 100 μM in 0.1 M HCl), BAY2416964 (Selleckchem #S8995, 1 μM in DMSO), or their respective vehicle solutions, fixed, and stained with Alizarin Red and Crystal Violet as described above for the BMSC-OB cultures.

Dual-energy X-ray absorptiometry

Mice were anesthetized using isoflurane and DXA was performed with a commercial system (Kubtec PARAMETER 3D cabinet, KUB Technologies). Whole body (excluding the head and ear tag) bone mineral content (BMC, grams) and bone mineral density (BMD, g/cm^2) were calculated using the manufacturer's analysis software (Kubtec Digimus). Femur midshaft, whole femur and L4-L6 lumbar vertebrae ROI measurements were defined in whole-mouse DXA images and analyzed with the manufacturer's software.

Micro-computed tomography

Femurs and lumbar vertebrae (L5) were scanned in a Bruker SkyScan 1272 micro-computed tomography (microCT) instrument (Bruker MicroCT). Before scanning, each sample was firmly wrapped in cotton gauze and packed into microcentrifuge tubes filled with 70% ethanol. Projection images were acquired using an image pixel size of 8.8-9.5 μm. The X-ray source was set to a voltage of 60-70 kVp at 142-166 μA. An aluminum filter was used for beam hardening correction. Each specimen was rotated 180° in 0.5° steps, with 4 averaged frames acquired per step using an integration time of 380 ms. A random movement setting of 10 was applied. Three hundred eighty-six projections were reconstructed into cross-sectional images using Bruker's NRecon software (ver. 1.7.4.6). A software beam hardening correction of 50% and a ring artifact reduction of 4 were applied across all specimens. Reconstructions were loaded into Bruker's CT-Analyzer (CTan) program for 2D and 3D morphometry. Using CTan, 2 representative volumes-of-interest (VOI) were defined in each femur for the analysis of trabecular and cortical bone. The femur trabecular VOI was selected based on the length of the femur and used the distal growth plate as a reference point, while the femur cortical VOI was established at the midpoint of the femur. The femoral trabecular bone was analyzed in the distal femoral metaphysis, within a region of interest spanning 100 slices beginning immediately above the primary spongiosa and extending proximally. Femoral cortical bone architecture was quantified in the mid-diaphysis, in a region of interest that was 50 slices in length, calculated from the femoral midpoint ±25 slices. Cortical bone ROIs were automatically selected using the periosteal perimeter as the outer boundary. Contouring for trabecular ROIs was performed manually, with borders drawn a few voxels away from the endocortical perimeter. Segmentation was performed using a global threshold of 80-255 Hounsfield Units. Bone architectural and density parameters were calculated using the manufacturer's software (CTAn) as previously described.[14,36]

Bone remodeling indices and BMAT

After microCT analysis, femurs were embedded in methyl methacrylate. Frontal sections were obtained from the distal third of each femur for trabecular bone analyses, whereas the mid-diaphysis of the femur was cross-sectioned at the femoral midpoint for cortical bone analyses. Histological sections were imaged and quantified for dynamic histomorphometry via fluorescent calcein labeling in the cortical and trabecular compartments. Tibias were decalcified in 15% ethylenediaminetetraacetic acid and embedded in paraffin prior to sectioning. Bone remodeling activity was quantified in the proximal tibia by static histomorphometry (H&E staining for osteoblasts with images at 10× original magnification, TRAP staining for osteoclasts with images at 20× original magnification). Trabecular bone static and dynamic histomorphometry analyses were completed on all trabeculae beginning at the growth plate and moving distally to 1/3 of the total bone length. Cortical bone dynamic and static histomorphometry were completed on cortical bone in the femoral diaphysis. Histological images were captured using an Olympus IX70 inverted microscope with a camera attachment (Qicam) or a Zeiss Axioscan 7 slide scanner. Bone marrow adipocyte area fraction (BMAd.Ar/M.Ar, %), bone marrow adipocyte density (N.BMAd/Ma.Ar, #/mm^2), trabecular osteoblast number (Tb.N.Ob/BS, #/mm), trabecular and cortical osteoclast number (Tb.N.Oc/BS and Ct.N.Oc/BS, #/mm), and the ratio of trabecular osteoclasts to osteoblasts (N.Oc/BS / N.Ob/BS) were quantified using Bioquant Osteo software (Bioquant Osteo).

Statistical analysis

All in vitro experiments were performed with a minimum of 3 independent biological replicates, and one-way ANOVA with

Fisher's LSD post hoc tests was used to compare the effects of KYN vs vehicle treatments. For in vivo or ex vivo datasets, the effects of genotype and sex on each property measured were investigated using 2-factor ANOVA with interaction, and pairwise comparisons were made between groups using Fisher's LSD post-hoc tests. Correlations between body mass and cortical bone properties were tested via linear regression. JMP Pro (v.18.0.2) was used for all statistical analyses, and a p-value of $p < .05$ was considered to be statistically significant. Box plots in the figures show median, quartiles, and outlier fences for each data set, where outlier fences represent first quartile −1.5*(interquartile range) and third quartile +1.5*(interquartile range). Bar charts show mean and standard error. Each biological replicate in box plots or bar charts is indicated by a separate data point, indicative of the sample size for each data set.

Results

Osx-Cre expression was confined to the bone in the adult-onset AhR CKO mouse model

Unlike our other models utilizing adult-onset Osx-Cre expression,[36] AhR mRNA expression in bone tissue was not significantly different between WT and AhR CKO animals (*data not shown*). This outcome was anticipated as the deletion of floxed exon 2 in the AhR allele of our conditional mouse model results in only minor changes in the mRNA sequence.[38] However, the deletion of exon 2 disrupts the binding of AhR to its cofactor AhR nuclear translocator (ARNT, also known as Hif1-beta), thereby preventing AhR's transcription factor activity.[37] PCR analysis of genomic DNA from various tissues from AhR CKO and WT littermate mice demonstrated specific recombination of the floxed AhR allele in bone tissues of CKO mice (demarrowed long bone and calvaria tissues). No recombination was observed in any other nonbone tissue tested nor was there evidence of Cre expression or recombination in Cre-negative WT littermates (Figure 1A). Additionally, no evidence of Cre-mediated DNA recombination, even in bone tissue, was observed when mice were maintained on a doxycycline chow diet (Figure 1B). These data confirm the skeletal specificity of AhR deletion and the efficacy of doxycycline-mediated suppression of Cre activity in our adult-onset AhR CKO model. In addition, we appreciate that several studies have reported the presence of Cre-driven skeletal phenotypes in the Osx1-Cre+ mouse line, even in the absence of recombination of a floxed gene.[39–41] However, using the doxycycline-driven adult-onset methodology as described above, we detected no evidence of a Cre-driven skeletal phenotype by micro-computed tomography in either male or female mice at 6 mo of age (Table S2).

Body mass was not different between WT and AhR CKO mice at 3 mo of age (while still on doxycycline; Figure 2A) or at 4.5 mo of age (ie, 6 wk of Cre activity; Figure 2B), but an interaction effect was detected between sex and genotype at 6 mo of age ($p = .0290$ for interaction), where female AhR CKO mice were significantly smaller than their female WT littermates ($p = .0375$ for post hoc), but no differences were seen between genotypes for males ($p = .4436$ for post hoc; Figure 2C).

Osx-Cre mediated AhR deletion protects osteoblasts from the harmful effects of KYN in vitro

To determine whether the effects of AhR deficiency in Osx-expressing cells affected cellular responses to the AhR ligand KYN, primary BMSC were subjected to osteogenic culture in the presence or absence of KYN in vitro. Consistent with previous reports,[6] BMSC-derived osteoblasts from 6-mo-old WT mice showed reduced mineralized matrix production in response to KYN treatment (Figure 3A). In contrast, BMSC-OB from KYN-treated AhR CKO cultures were protected against the harmful effects of KYN, as these cultures did not demonstrate a significant reduction in Alizarin Red staining with KYN treatment. Neither genotype, nor KYN treatment affected the growth of BMSC-derived osteoblast colonies, as shown by Crystal Violet staining (Figure 3B), and the harmful impact of KYN on mineralized matrix production by WT but not AhR CKO BMSC-OB persisted after normalization to crystal violet staining (Figure 3C).

Conditioned medium was collected from AhR CKO and WT BMSC-OB cultures derived from 6-mo-old mice and analyzed in Luminex-based assays to quantify levels of RANKL, M-CSF, and OPG released by the primary BMSC-OB. Interestingly, RANKL levels were elevated in the conditioned medium from AhR CKO osteoblasts ($p = .0309$ for genotype), and this trend tended to be stronger in cells isolated from male mice ($p = .0514$ for interaction; Figure 4A). M-CSF levels were not affected by genotype or sex (Figure 4B), and OPG levels, while lower in female than male cultures ($p = .0035$ for sex), were not affected by genotype (Figure 4C). However, the ratio of OPG to RANKL, representing the balance of anti- to pro-osteoclastogenic signaling from the BMSC-OB, was lower in the conditioned medium from AhR CKO as compared to WT osteoblasts ($p = .0102$ for genotype, Figure 4D).

Immortalized MC3T3 cells were used to further investigate the impact of AhR-mediated signaling across various stages of osteoblastic differentiation (Figure 5A) using a pharmacological AhR antagonist (BAY2416964). Quantification of matrix production via Alizarin Red staining revealed that the AhR ligand KYN induced the greatest suppression of mineralized matrix production when it was present during days 7-14 of osteoblastic differentiation (Figure 5B and C), although the magnitude of KYN's impact on osteoblastic matrix formation was lower than if KYN was present during the entire 21-d time course of osteogenic differentiation (Figure S1A and B). This effect of KYN during the days 7-14 culture window was rescued by co-treatment with the AhR antagonist BAY2416964, as cells treated with KYN + BAY2416964 produced significantly more matrix than cells treated with KYN alone (Figure 5B). Cell growth, as shown by Crystal Violet staining, was not affected by KYN or AhR inhibition at any stage of differentiation (Figure S1C), and trends for effects of KYN and BAY2416964 on matrix production by MC3T3 cells during day 7-14 of culture tended to persist after normalizing matrix formation to colony area (Figure S1D), although BAY2416964 was unable to significantly rescue KYN effects when KYN was present for the entire D0-D21 time course (Figure S1A, E, and F).

AhR CKO mice developed sexually dimorphic, compartment-specific skeletal phenotypes

Dual-energy x-ray absorptiometry analysis was completed at 4.5 and 6 mo of age (i.e., ∼6 and 12 wk of CKO) and showed no impact of Osx-Cre-mediated AhR deletion on whole body bone mineral density (BMD; $p > .1355$ for genotype, Figure S2A and C) or bone mineral content (BMC; $p > .2914$ for genotype, Figure S2B and D). Region of interest DXA analysis of the lumbar vertebrae (Figure S2E-H) showed no effect of AhR CKO in either age group ($p > .4588$ for genotype).

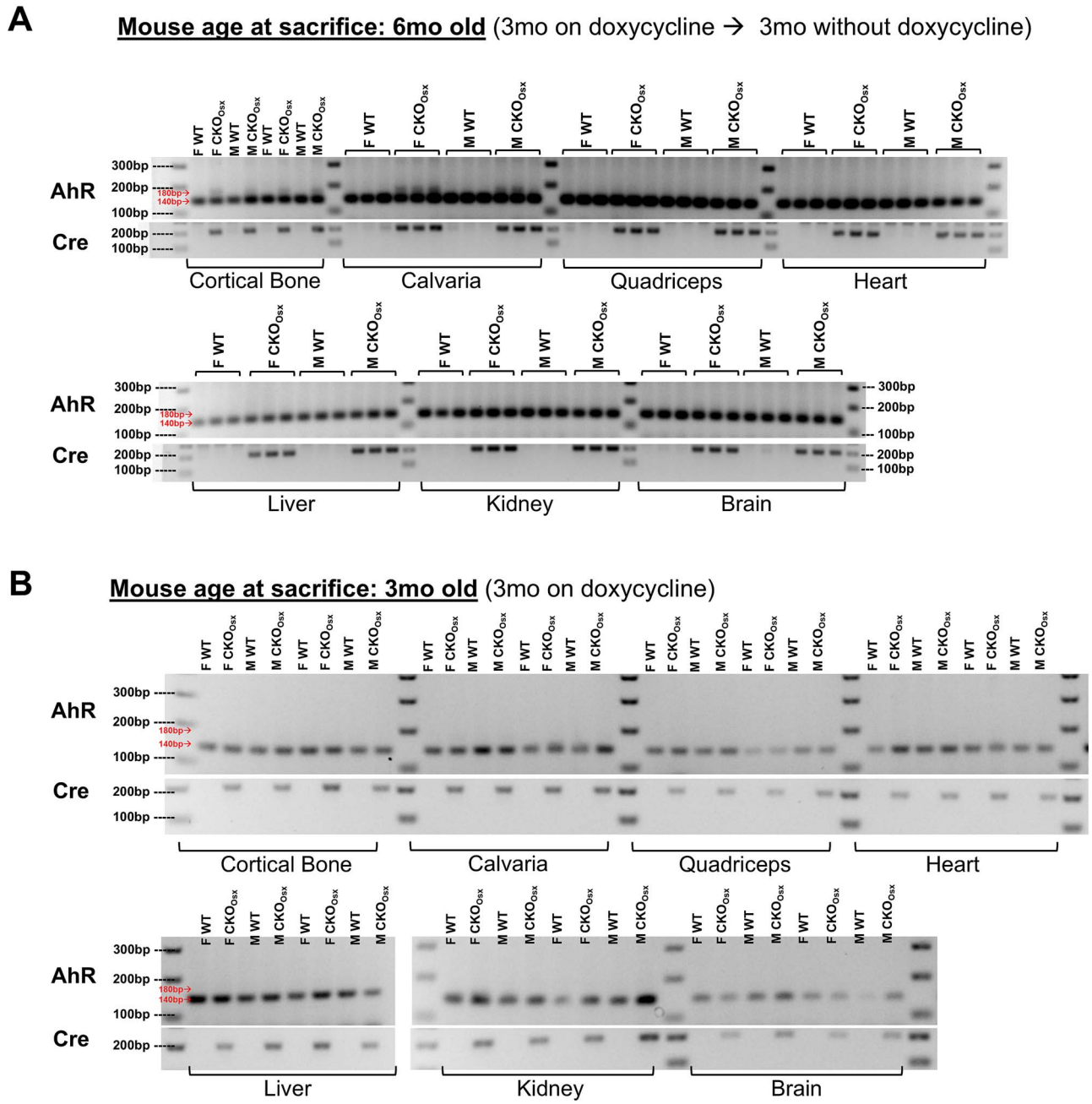

Figure 1. Osx-Cre expression was confined to bone in the adult-onset AhR CKO mouse model. Recombination of the floxed allele (evidenced by the creation of a 180 bp band) occurred only in cortical bone (demarrowed long bone tissue) and calvarial bone of AhR CKO mice, and was not seen in other tissues at 6 mo of age (A). Cre activity was effectively suppressed by doxycycline, as no DNA recombination was seen at 3 mo of age in any tissue (including bone) while mice were receiving doxycycline-supplemented chow (B). Each lane represents a separate biological sample (ie, independent mice).

Mid-femoral diaphysis (Figure S2I-L) and whole femur (Figure S2M-P) DXA analyses revealed no changes at 4.5 mo of age ($p > .0655$ for genotype), however at 6 mo of age, a significant interaction between sex and genotype occurred ($p < .0353$ for interaction) where male (but not female) AhR-CKO mice had increased BMD at both mid-shaft (Figure S2K) and whole femur (Figure S2O) ROI compared to sex-matched WT littermates.

High-resolution microCT analysis was performed to assess the impact of AhR conditional deletion on bone architecture at 4.5 mo (Table 1) and 6 mo (Table 2) of age. At 4.5 mo of age, both male and female AhR CKO mice showed greater trabecular bone mass than WT littermates in the distal femoral metaphysis, evidenced by a reduction in trabecular separation ($p < .0001$ for genotype), increased trabecular number ($p = .0190$ for genotype), and a strong trend for increased trabecular bone volume fraction ($p = .0508$ for genotype) as compared to sex-matched WT littermates. Cortical bone mass showed an interaction between genotype and sex for several properties, with lower cortical bone tissue area and cortical bone polar moment of inertia but greater cortical bone volume fraction (Ct.BV/TV) in male AhR CKO mice as compared to sex-matched littermates, whereas no differences were observed between genotypes for females

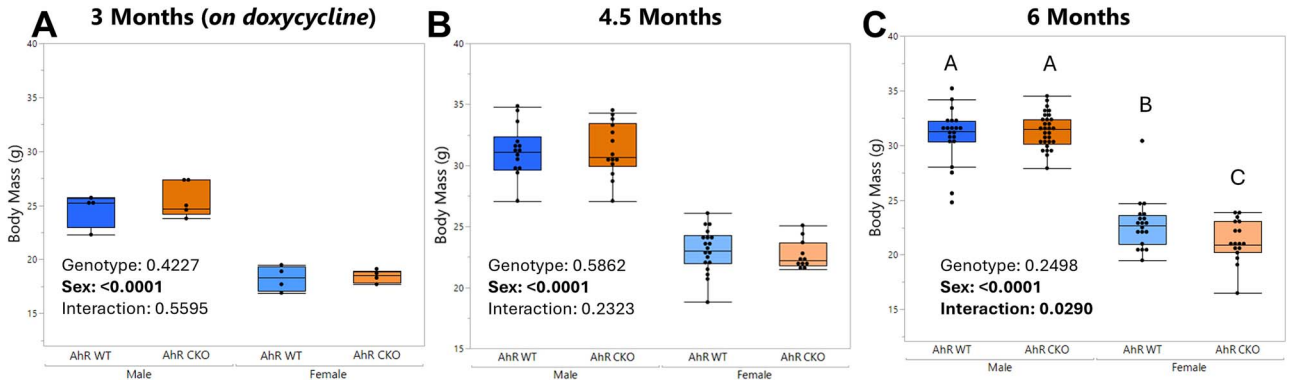

Figure 2. Body masses were not different between AhR CKO mice and WT littermates at 3 mo (A) or 4.5 mo of age (B); however, female AhR CKO mice were significantly smaller than WT littermates at 6 mo of age (C). Box plots show median, quartiles, and outlier fences for each group, where outlier fences represent first quartile −1.5* (interquartile range) and third quartile +1.5* (interquartile range), and each black circle represents 1 mouse. Groups with different superscript letters are significantly ($p < .05$) different from one another as shown by post-hoc testing.

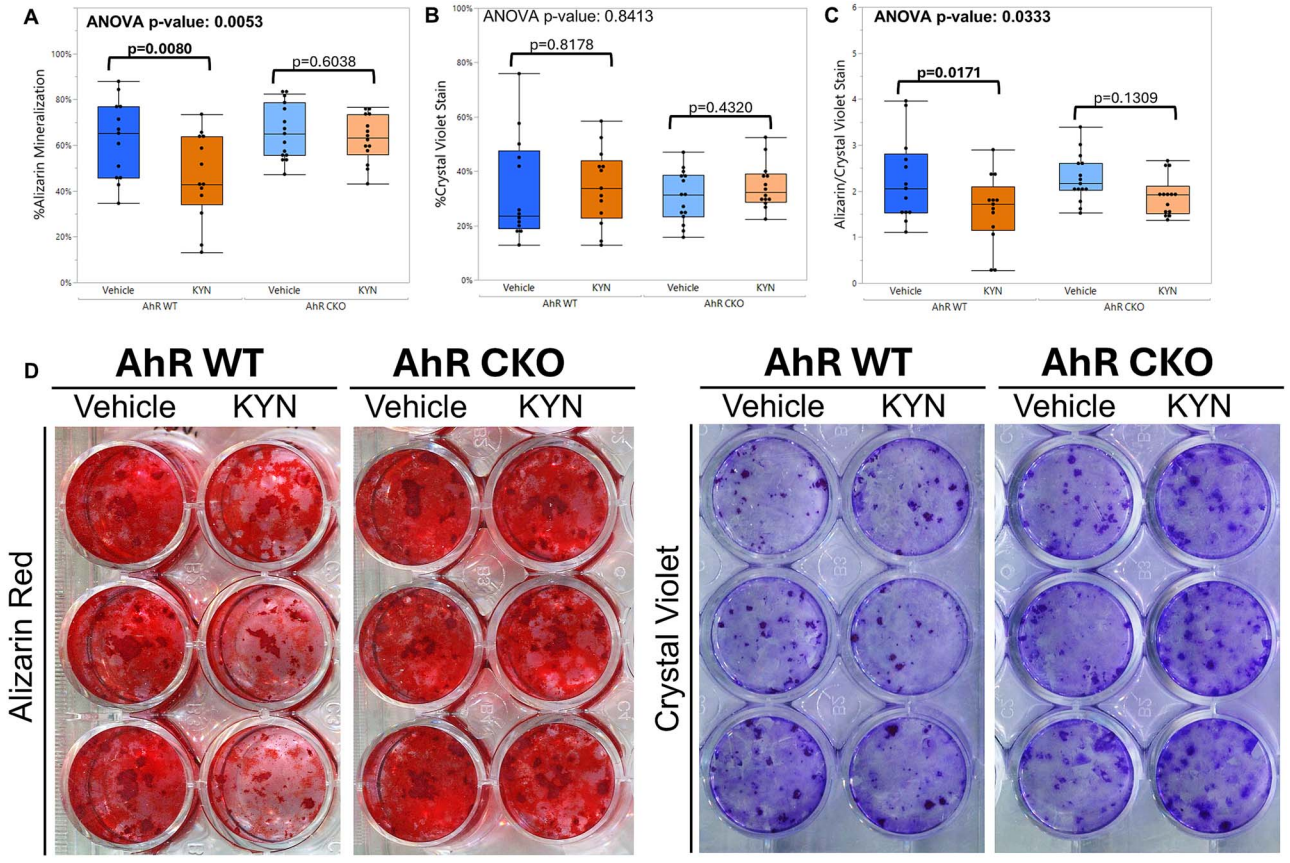

Figure 3. While WT BMSC-OB cultures demonstrated reduced mineralized matrix production in response to KYN treatment, AhR CKO BMSC-OB were protected from this effect (A). Neither KYN nor AhR genotype affected cell growth as shown by crystal violet staining of colony formation (B). The negative impact of KYN on mineralized matrix production by WT but not AhR CKO osteoblasts persisted after normalizing the matrix area to the cell colony area (C). Representative images of staining are shown in panel D. Box plots show median, quartiles, and outlier fences for each group, where outlier fences represent first quartile −1.5* (interquartile range) and third quartile +1.5* (interquartile range), and each black circle represents 1 biological replicate cell culture.

(Table 1). Other cortical bone properties were not affected by genotype (Table 1).

At 6 mo of age, the increased trabecular bone mass phenotype observed in younger animals persisted, with AhR CKO mice demonstrating increased trabecular number ($p = .0001$ for genotype) and decreased trabecular separation ($p < .0001$ for genotype), as compared to WT littermates, however a significant reduction in trabecular thickness in the AhR CKO mice was also seen in both sexes ($p = .0020$ for genotype; Table 2). Interestingly, the cortical bone mass phenotype seen in males at younger ages resolved by 6 mo of age, with mid-femoral cortical bone showing no differences between male AhR CKO and WT males at 6 mo of age. The female AhR CKO mice demonstrated a significant reduction in cortical bone tissue mineral density (TMD), cortical bone area, Ct.BV/TV, cortical bone polar moment of inertia, and cortical

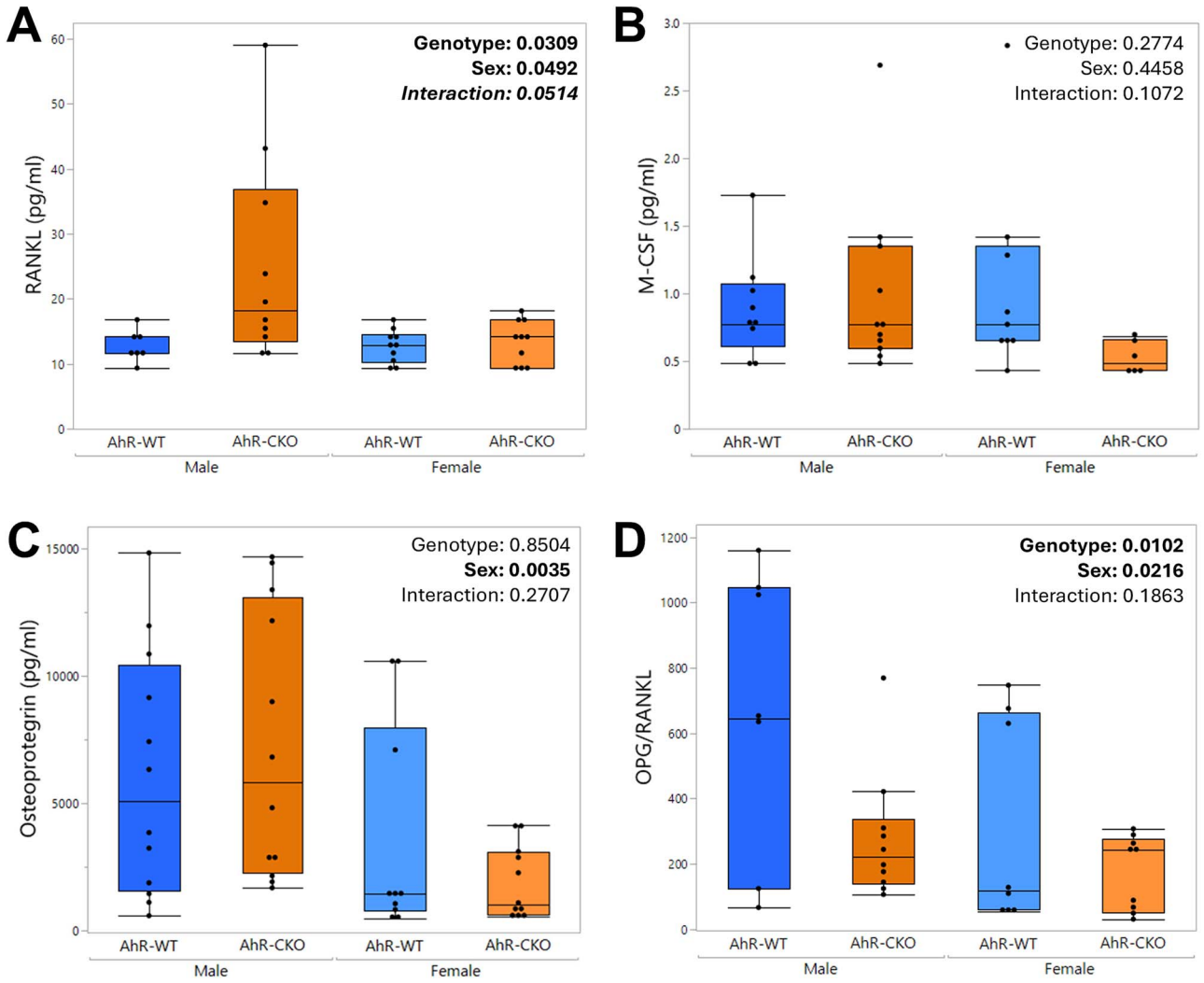

Figure 4. Conditioned cell culture medium was collected from BMSC-OB cultures of 6-mo-old mice at D7 (D6-D7 culture period) and D14 (D13-D14 culture period) and analyzed for protein expression using Luminex-based technology. Released levels of RANKL (A) were elevated in the AhR CKO as compared to WT BMSC-OB cultures, particularly for male mice. M-CSF levels (B) were not affected by sex or genotype, whereas OPG levels (C) were lower in female than male cultures but were not affected by genotype. Interestingly, the ratio of OPG to RANKL, representing the balance of anti- to pro-osteoclastogenic signaling from osteoblast-lineage cells, was significantly lower in the AhR CKO as compared to WT BMSC-OB cultures for both sexes. Box plots show median, quartiles, and outlier fences for each group, where outlier fences represent first quartile −1.5* (interquartile range) and third quartile +1.5* (interquartile range), and each black circle represents 1 biological replicate cell culture.

bone thickness as compared to female WT littermates at 6 mo of age (Table 2), consistent with the smaller body size in female CKO mice observed at this age (Figure S3).

AhR CKO mice showed altered bone remodeling activity

Histological bone remodeling indices were analyzed in 4.5- and 6-mo-old mice to elucidate the cellular changes driving the skeletal architectural differences seen via microCT. Periosteal bone mineralizing surface, mineral apposition rate, and bone formation rate were not affected by Osx-Cre-mediated AhR deletion at either age ($p > .5443$ for genotype; Figure 6A-H). On the endocortical surface, endosteal mineralizing surface was lower in female AhR CKO mice compared to sex-matched WT littermates at 4.5 mo of age (Figure 6I), but endosteal BFR (Figure 6J) and endosteal MAR (Figure 6K) were unaffected, and no genotype-related differences nor interaction effects were seen at 6 mo of age (Figure 6M-O), except for mild trends for reduced endosteal mineralizing surface ($p = .0950$ for genotype) and endosteal BFR ($p = .0651$ for genotype) in AhR CKO mice from both sexes.

Despite the high trabecular bone mass seen in AhR CKO mice at 4.5 mo of age, no significant differences were observed in dynamic indices of trabecular bone formation at this age ($p > .1693$ for genotype, Figure 6Q-T). By 6 mo of age, although trabecular bone mass remained higher in AhR CKO mice, trabecular bone mineralizing surface and bone formation rate were unchanged, whereas trabecular bone mineral apposition rate was decreased in AhR CKO mice as compared to WT littermates ($p = .0190$ for genotype), with a trend for this difference between genotypes to be stronger in female than in male mice ($p = .0730$ for interaction; Figure 6U-W).

In terms of static histomorphometry, no differences were seen in trabecular osteoblast number between AhR CKO and WT mice at 4.5 mo of age ($p = .2475$ for genotype, Figure 7A and B), but trabecular osteoblast numbers were significantly greater in male AhR CKO mice at 6 mo of age as compared

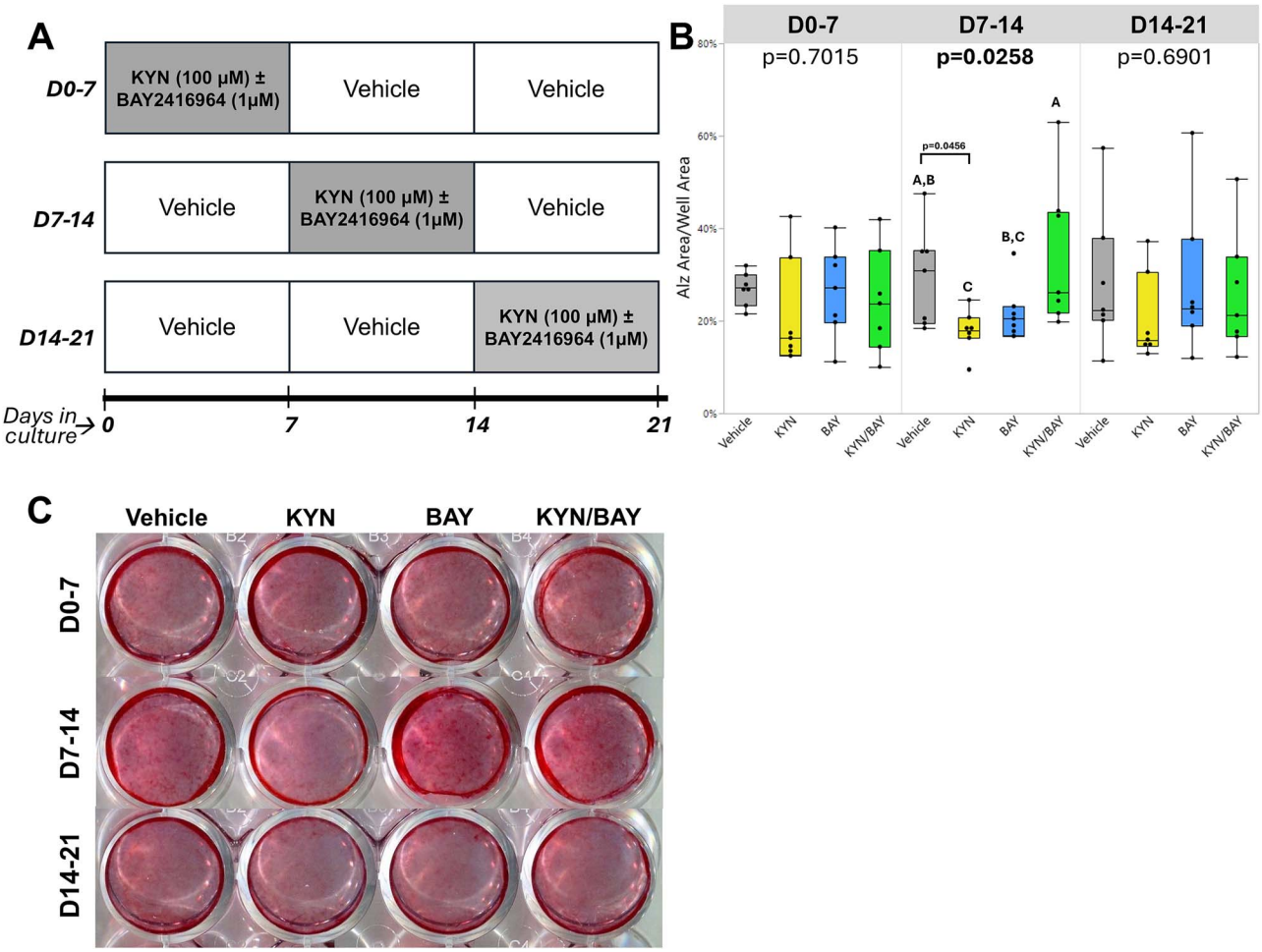

Figure 5. In vitro assays of MC3T3 cells treated for 7-d windows (A) during a 21-d osteogenic differentiation time course with KYN or the AhR inhibitor BAY2416964. Kynurenine treatment exerted the most notable negative effects on matrix production during days 7-14 of culture, and this effect was rescued by BAY2416964 (B). Representative images of Alizarin Red staining are shown in panel C. Box plots show median, quartiles, and outlier fences for each group, where outlier fences represent first quartile −1.5* (interquartile range) and third quartile +1.5* (interquartile range), and each black circle represents 1 biological replicate cell culture. One-way ANOVA *p*-values are shown above each culture window, and groups with different superscript letters are significantly ($p < .05$) different from one another as shown by post-hoc testing.

Table 1. MicroCT parameters of female and male AhR-CKO and AhR-wild-type (AhR-WT) mice femurs at 4.5 mo of age.

Parameter	Female AhR-WT ($n = 13$)	Female AhR-CKO ($n = 6$)	Male AhR-WT ($n = 7$)	Male AhR-CKO ($n = 11$)	*p*-values		
					Sex	Genotype	Interaction
Tb. BV/TV (%)	2.087 ± 0.213	3.299 ± 0.514	11.495 ± 0.607	12.609 ± 0.742	<.0001	.0508	.9327
Tb. Th (mm)	$0.036^{B} \pm 0.005$	$0.040^{B} \pm 0.001$	$0.051^{A} \pm 0.001$	$0.047^{A} \pm 0.002$	<.0001	.9941	.0549
Tb. Sp (mm)	0.311 ± 0.006	0.278 ± 0.009	0.226 ± 0.005	0.200 ± 0.004	<.0001	<.0001	.5936
Tb. N (#/mm)	0.575 ± 0.047	0.825 ± 0.117	2.249 ± 0.119	2.664 ± 0.110	<.0001	.0019	.4057
Ct. TMD (g/cm^3)	1.435 ± 0.033	1.414 ± 0.046	1.411 ± 0.041	1.343 ± 0.027	.2148	.2395	.5339
Ct.T.Ar (mm^2)	$1.654^{C} \pm 0.034$	$1.650^{C} \pm 0.033$	$2.329^{A} \pm 0.061$	$2.062^{B} \pm 0.052$	<.0001	.0096	.0116
Ct. B.Ar (mm^2)	0.766 ± 0.011	0.749 ± 0.025	0.988 ± 0.026	0.950 ± 0.026	<.0001	.2185	.6218
Ct. BV/TV (%)	$46.412^{A} \pm 0.535$	$45.366^{A} \pm 0.714$	$42.463^{B} \pm 0.759$	$45.263^{A} \pm 0.474$	.0028	.1716	.0043
Ct. MMI_{polar} (mm^4)	$0.323^{C} \pm 0.012$	$0.319^{C} \pm 0.018$	$0.611^{A} \pm 0.030$	$0.506^{B} \pm 0.025$	<.0001	.0207	.0322
Ct.M.Ar (mm^2)	0.696 ± 0.070	0.732 ± 0.102	1.001 ± 0.127	1.019 ± 0.083	.0039	.7771	.9273
Ct.Th (mm)	0.177 ± 0.002	0.172 ± 0.004	0.183 ± 0.005	0.184 ± 0.004	.0205	.6001	.3801

Parameter means and SE are presented. The *p*-values for variables and interactions assessed by 2-factor ANOVA are shown. For properties where a significant interaction was detected between sex and genotype, group means with different superscript letters are significantly ($p < .05$) different from one another, as indicated by post hoc testing. Abbreviations: Ct. B.Ar, cortical bone area; Ct. BV/TV, cortical bone volume fraction; Ct. MMI_{polar}, cortical bone polar moment of inertia; Ct. M.Ar, cortical bone marrow area; Ct. T.Ar, cortical bone tissue area; Ct. Th, cortical bone thickness; Ct. TMD, cortical bone tissue mineral density; Tb. BV/TV, trabecular bone volume fraction; Tb. N, trabecular number; Tb. Sp, trabecular separation; Tb. Th, trabecular thickness.

to WT littermates ($p = .0274$ for interaction; Figure 7C and D). Trabecular osteoclast numbers tended to be suppressed in AhR CKO mice of both sexes at 4.5 mo of age ($p = .0555$ for genotype) but this was only significant for male AhR CKO mice by 6 mo of age ($p = .0456$ for interaction; Figure 7E-H). Consistent with the high trabecular bone mass phenotype, the

Table 2. MicroCT parameters of female and male AhR-CKO and AhR-wild-type (AhR-WT) mice femurs at 6 mo of age.

Parameter	Female AhR-WT ($n = 16$)	Female AhR-CKO ($n = 16$)	Male AhR-WT ($n = 20$)	Male AhR-CKO ($n = 29$)	p-values		
					Sex	Genotype	Interaction
Tb. BV/TV (%)	5.008 ± 0.410	6.474 ± 0.593	16.642 ± 1.192	18.357 ± 0.935	<.0001	.1084	.8991
Tb. Th (mm)	0.053 ± 0.001	0.047 ± 0.001	0.061 ± 0.002	0.056 ± 0.001	<.0001	.0020	.6398
Tb. Sp (mm)	$0.365^{A} \pm 0.008$	$0.320^{B} \pm 0.008$	$0.237^{C} \pm 0.004$	$0.214^{D} \pm 0.004$	<.0001	<.0001	.0562
Tb. N (#/mm)	0.955 ± 0.079	1.366 ± 0.107	2.682 ± 0.137	3.204 ± 0.100	<.0001	.0001	.6328
Ct. TMD (g/cm^3)	$1.653^{A} \pm 0.036$	$1.471^{A,B} \pm 0.090$	$1.404^{B} \pm 0.056$	$1.495^{B} \pm 0.048$	.0610	.4387	.0236
Ct.T.Ar (mm^2)	1.742 ± 0.030	1.639 ± 0.021	2.282 ± 0.055	2.301 ± 0.032	<.0001	.2945	.1279
Ct. B.Ar (mm^2)	$0.811^{B} \pm 0.016$	$0.725^{C} \pm 0.015$	$0.931^{A} \pm 0.018$	$0.964^{A} \pm 0.013$	<.0001	.1020	.0004
Ct. BV/TV (%)	$46.560^{A} \pm 0.466$	$44.221^{B} \pm 0.682$	$40.985^{C} \pm 0.646$	$42.001^{C} \pm 0.530$	<.0001	.2832	.0076
Ct. MMI$_{polar}$ (mm^4)	$0.361^{B} \pm 0.013$	$0.306^{C} \pm 0.009$	$0.572^{A} \pm 0.022$	$0.593^{A} \pm 0.015$	<.0001	.3301	.0278
Ct.M.Ar (mm^2)	0.931 ± 0.018	0.914 ± 0.015	1.351 ± 0.043	1.337 ± 0.027	<.0001	.6213	.9548
Ct.Th (mm)	$0.181^{A} \pm 0.003$	$0.165^{B} \pm 0.004$	$0.175^{A} \pm 0.002$	$0.178^{A} \pm 0.002$	.2205	.0202	.0012

Parameter means and SE are presented. The p-values for variables and interactions assessed by 2-factor ANOVA are shown. For properties where a significant interaction was detected between sex and genotype, group means with different superscript letters are significantly ($p < .05$) different from one another, as indicated by post hoc testing. Abbreviations: Ct. B.Ar, cortical bone area; Ct. BV/TV, cortical bone volume fraction; Ct. M.Ar, cortical bone marrow area; Ct. MMI$_{polar}$, cortical bone polar moment of inertia; Ct. T.Ar, cortical bone tissue area; Ct. Th, cortical bone thickness; Ct. TMD, cortical bone tissue mineral density; Tb. BV/TV, trabecular bone volume fraction; Tb. N, trabecular number; Tb. Sp, trabecular separation; Tb. Th, trabecular thickness.

ratio of trabecular osteoclasts to osteoblasts was significantly lower in AhR CKO as compared to WT mice at 4.5 mo of age ($p = .0262$ for genotype; Figure 7I) suggesting a positive net bone remodeling balance that may have promoted increased trabecular bone mass. By 6 mo of age, the ratio of osteoclast to osteoblast numbers was no longer significantly different between genotypes ($p = .9671$ for genotype; Figure 7J). In the cortical bone compartment, an interaction between genotype and sex was observed at 4.5 mo of age where endosteal cortical bone osteoclast numbers tended to be lower in male AhR CKO mice as compared to WT littermates (Figure 7K and L, $p = .0548$ for post hoc), consistent with their higher Ct.BV/TV seen by microCT. This trend was not seen in 6-mo-old animals (Figure 7M and N) and may reflect the propensity of AhR CKO osteoblasts to favor pro-osteoclastogenic signaling (i.e., lower OPG to RANKL ratio) by 6 mo of age as shown in analyses of conditioned medium (Figure 4).

As we previously observed that the AhR ligand KYN promoted increased bone marrow adiposity,[6] we also quantified BMAT in the AhR CKO and WT littermate mice. Neither bone marrow adipocyte density (Figure 7O) nor adipocyte area fraction (Figure 7P) were altered in AhR CKO mice at 4.5 mo of age ($p > .1834$ for genotype), however, a trend was noted at 6 mo of age where bone marrow adipocyte area fraction tended to be higher in female AhR CKO mice as compared to sex-matched littermates ($p = .0716$ for interaction, Figure 7Q and R).

Discussion

While previous research supports a role for KYN as a causative factor in musculoskeletal frailty,[4,6,13,14] and impaired osteoblastic bone formation,[3,6,7,12,13] the in vivo molecular mediator of KYN-induced osteoblast dysfunction has not yet been reported. Our findings suggest that conditional deletion of AhR in Osx-expressing cells protects against KYN-induced reductions in osteoblastic matrix production but confers compartment-specific and sexually dimorphic skeletal phenotypes. These observations underscore the nuanced, context-dependent functions of AhR in bone biology while providing important insights into the role of AhR in skeletal homeostasis.

Although the limitations of the Osx-Cre model have been widely reported,[39–42] our study confirmed that Osx-Cre-driven deletion of AhR was specific to skeletal tissues in the doxycycline-suppressed, adult-onset CKO model. This specificity was demonstrated by the absence of Cre-mediated recombination in non-bone tissues and in Cre-negative controls. Furthermore, doxycycline effectively suppressed Cre activity in this model as evidenced by a lack of exon 2 deletion in the AhR allele in all mice (including Cre+ animals) while maintained on doxycycline-supplemented chow. Moreover, we did not detect any skeletal architecture differences in Cre + WT animals at 6 mo of age as compared to Cre-negative WT mice (Table S2). Although DXA-based bone density metrics showed few differences between AhR WT and AhR CKO mice, high-resolution microCT analysis revealed a high trabecular bone mass phenotype in AhR CKO mice by 4.5 mo of age, corresponding to approximately 6 wk of AhR conditional deletion. Interestingly, although the high trabecular bone mass phenotype of AhR CKO mice persisted at 6 mo of age, it was accompanied by reduced trabecular thickness, suggesting that long-term AhR deficiency may impact trabecular structure differently over time. Histomorphometry analyses were utilized to define cellular contributions to the AhR-mediated skeletal phenotypes observed. Dynamic histomorphometry analyses revealed that the high trabecular bone mass observed in AhR CKO mice at 4.5 mo of age was likely not driven by increased bone formation rates; this is consistent with in vitro studies with primary BMSC-OB, where AhR CKO cultures did not notably produce more mineralized matrix as compared to WT cultures (Figure 3). Instead, a reduction in trabecular osteoclast numbers and a lower osteoclast-to-osteoblast ratio as compared to wildtype littermates observed in histological analyses suggest decreased bone resorption as a contributing factor in the AhR CKO-mediated trabecular bone phenotype. Future studies aimed at understanding the role of AhR in the osteoblast-mediated regulation of osteoclastogenesis are warranted to better understand the mechanisms driving the trabecular bone phenotype in AhR CKO mice.

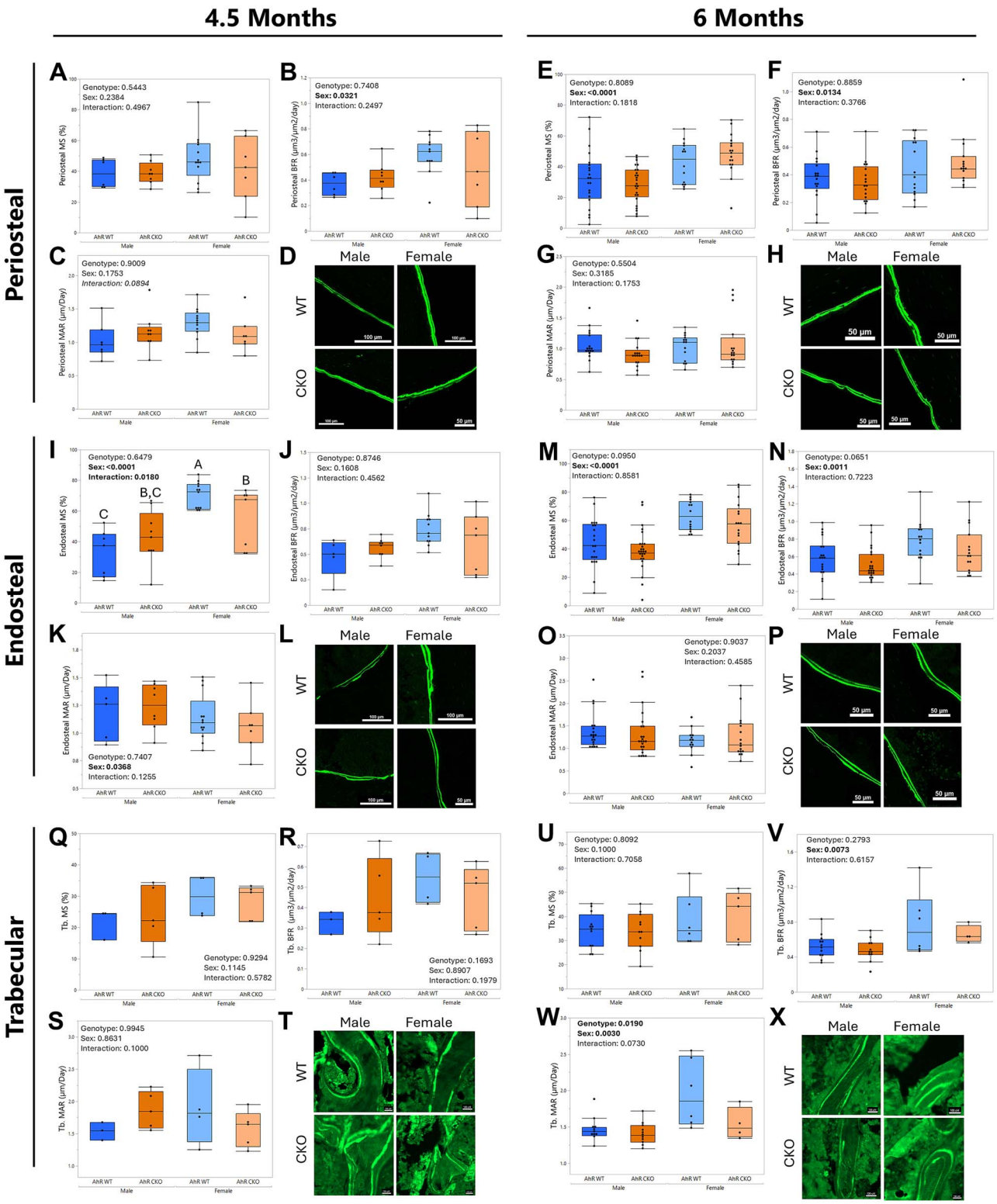

Figure 6. Dynamic histomorphometry revealed a compartment-specific remodeling phenotype in AhR CKO mice, with few changes in cortical bone metrics but decreases in metrics of trabecular bone mineralization at 6 mo of age. Periosteal bone formation metrics showed no changes at 4.5 mo (A-D) or 6 mo of age (E-H). At 4.5 mo of age, the endosteal mineralizing surface was lower in female CKO mice as compared to WT littermates, but no differences were seen in MAR or BFR for females or in any metrics for males (I-L), and these differences were resolved by 6 mo of age (M-P). Trabecular bone dynamic histomorphometry revealed no changes at 4.5 mo of age (Q-T), while at 6 mo of age, trabecular mineral apposition rate was decreased in AhR CKO mice (W) although BFR and mineralizing surface were unchanged (U, V, X). Representative images from 1 mouse per group are shown in panels D, H, L, P, T, and X. Box plots show median, quartiles, and outlier fences for each group, where outlier fences represent first quartile −1.5* (interquartile range) and third quartile +1.5* (interquartile range), and each black circle represents 1 mouse. Groups with different superscript letters are significantly ($p < .05$) different from one another as shown by post-hoc testing.

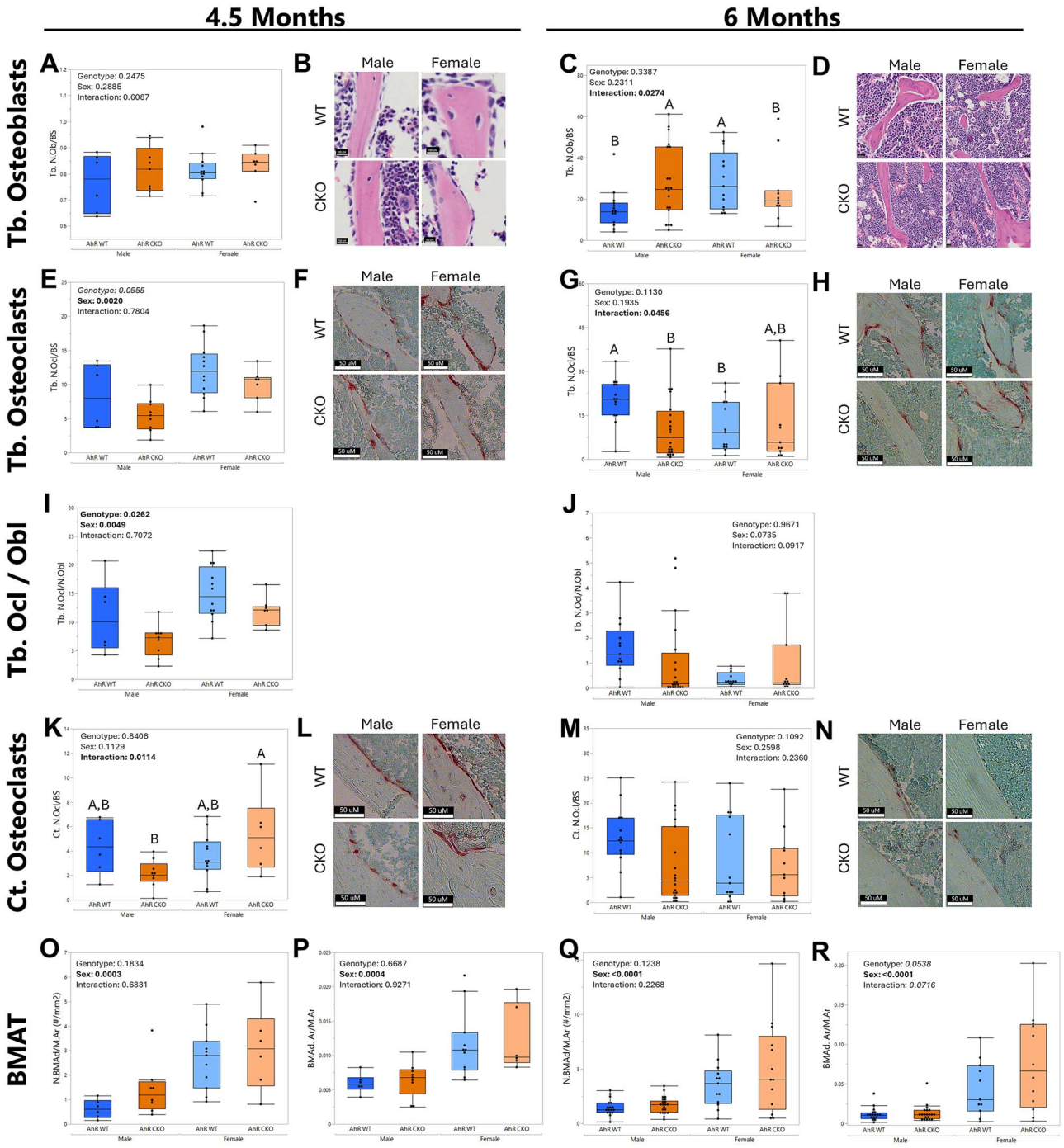

Figure 7. AhR CKO mice showed a positive net balance between osteoclasts and osteoblasts at 4.5 mo of age, suggestive of more bone formation than bone resorption consistent with the high trabecular bone mass phenotype seen by microCT at this age. Static histomorphometry analysis of the trabecular osteoblasts showed no changes due to AhR deletion at 4.5 mo (A, B) but a sexually dimorphic effect of AhR deletion at 6 mo of age, with an increase in osteoblast number in AhR CKO males as compared to male WT littermates but a significant decrease in AhR CKO females as compared to female WT littermates (C, D). At 4.5 mo of age, trabecular osteoclasts tended to be reduced in AhR CKO animals (E, F); this trend was maintained in males, but not females, at 6 mo (G, H). The relative ratio of osteoclasts to osteoblasts showed a reduction in CKO animals at 4.5 mo (I), consistent with the high trabecular bone mass phenotype, although this trend resolved by 6 mo of age (J). Cortical osteoclasts were reduced in male AhR CKO mice at 4.5 mo (K, L), but this also resolved by 6 mo of age (M, N). BMAT was unchanged at either rage (O-R), although female AhR CKO mice showed a mild trend toward increased bone marrow adipocyte area fraction (R). Representative images from 1 mouse per group are shown in panels B, D, F, H, L, and N. Box plots show median, quartiles, and outlier fences for each group, where outlier fences represent first quartile −1.5* (interquartile range) and third quartile +1.5* (interquartile range), and each black circle represents 1 mouse. Groups with different superscript letters are significantly ($p < .05$) different from one another as shown by post-hoc testing.

In the cortical bone compartment, AhR's effects were sexually dimorphic. Male AhR CKO mice exhibited greater Ct.BV/TV at 4.5 mo of age as compared to WT littermates, consistent with a trend for decreased cortical bone osteoclasts, although this phenotype resolved by 6 mo of age despite cortical bone BMD remaining higher in the male AhR

CKO mice as shown by DXA. In contrast, female AhR CKO mice demonstrated reduced cortical bone mass as compared to WT females by 6 mo of age. These results raise the possibility that AhR activity may interact with sex hormones or other systemic factors to influence cortical bone homeostasis in a time- and compartment-dependent manner. AhR and the estrogen receptor (ER) have been reported to interact in a multitude of ways on a molecular level,[43] including in osteoblasts where the AhR-activating ligand 3-methylcholanthrene (3-MC) promoted aromatase-dependent increases in cell proliferation in osteoblastic hFOB and MG-63 cells in a manner that could be prevented by the AhR inhibitor CH-223191.[44] However, we did not see any impact of KYN or AhR inhibition by BAY2416964 on the proliferative behavior of primary BMSC-Ob or MC3T3 cells as shown by Crystal Violet staining (Figures 3 and 5), and it is also worth noting that Osx-Cre-mediated AhR deletion also reduced overall body size in female AhR CKO mice at 6 mo of age (as shown by decreased body mass; Figure 2C and Figure S3). The impetus for this change in body size despite AhR deletion being confined to skeletal tissues in our adult-onset CKO model, and the potential relationship between altered body size and the cortical bone mass phenotype of AhR CKO female mice (Figure S3) is not yet known but will be explored in future studies. The resolution of the high cortical bone mass phenotype of AhR CKO males and the onset of a low cortical bone mass phenotype in AhR CKO females at 6 mo may have been influenced by the propensity of AhR CKO osteoblasts to favor pro-osteoclastogenic signaling (ie, lower OPG to RANKL ratio) by 6 mo of age as shown in analyses of conditioned medium from the BMSC-OB cultures. However, since histological metrics of cortical bone osteoclast abundance were unchanged at 6 mo of age, this possibility will require further study.

Consistent with prior reports, KYN treatment impaired mineralized matrix production in BMSC-derived osteoblast cultures from WT mice. However, this harmful effect was absent in osteoblasts from AhR CKO mice, supporting the hypothesis that AhR is a critical mediator of KYN's inhibitory effects on osteoblasts. Importantly, this protection occurred without affecting cell proliferation, indicating that AhR deletion specifically mitigates the downstream effects of KYN on osteoblast differentiation and matrix production. Notably, AhR-deficient osteoblasts did not appear to produce more matrix than their WT counterparts under baseline conditions, suggesting that AhR's role in osteoblast function might not occur in a cell-autonomous fashion. Further support for AhR's mediation of KYN's effects was provided by pharmacological inhibition of AhR in MC3T3 cells. Co-treatment with an AhR antagonist rescued the KYN-induced reduction in mineralized matrix production, confirming that AhR's activity contributes to KYN's deleterious effects during osteoblastic differentiation. These findings implicate AhR as a molecular target for mitigating age-related bone loss associated with elevated KYN levels.

While studies presented here represent a critical first step in understanding the role of osteoblastic AhR in adult skeletal maintenance, it is important to note that expression levels of the AhR ligand KYN are quite low in young adults, and only substantially increase in the circulation and in the skeletal niche at advanced ages,[6,7] such as in humans where serum KYN levels are highest in frail as compared to robust or prefrail elderly patients.[45] Therefore, the skeletal benefit of deleting or inhibiting the proposed receptor mediating KYN's negative effects in bone may become more evident with age; future studies will examine the skeletal phenotypes of aged AhR CKO mice (when KYN levels are naturally higher), and may also directly test whether deletion of AhR in Osx-expressing cells protects mice against the harmful skeletal effects of exogenous KYN treatment. In addition, the phenotypical differences induced by AhR deficiency between the trabecular and cortical bone compartments observed here warrant further study to determine whether the impacts of AhR-mediated signaling differ between these sites. Supporting this possibility, a recent publication[46] utilized bulk RNA-seq to compare gene expression profiles between cortical and trabecular bone sites in female mice, and these datasets showed that expression levels of AhR, the AhR target gene Cyp1b1, and the gene Slc7a5/LAT1 (a transporter capable of moving tryptophan and its metabolites like KYN[24] across the cell membrane) were more highly expressed in cortical bone than in trabecular bone (fold change in cortical vs trabecular bone, all $p < .001$: AhR = +2.31 fold, Cyp1b1 = +2.38 fold, Slc7a5/LAT1 = +2.50 fold; Table S3 in the cited publication). Accordingly, it is possible that AhR-mediated signaling affects cortical and trabecular bone in different ways, but this hypothesis will need to be directly tested in future studies.

In conclusion, the current study provides compelling evidence that expression of AhR in Osx-lineage cells plays a critical role in bone, acting as a mediator of endogenous ligand (KYN)-induced osteoblast dysfunction while also influencing bone remodeling activity in a compartment- and sex-specific manner. These findings highlight the complexity of AhR signaling in bone biology while also supporting its potential as a therapeutic target for conditions associated with elevated KYN levels, such as osteoporosis and musculoskeletal frailty. Future studies will define the mechanisms underlying the sexually dimorphic effects of AhR deletion and its interaction with systemic factors like sex hormones and inflammation. Understanding the ligand-specific and context-dependent effects of AhR signaling will be critical for developing targeted therapies that exploit AhR's protective potential while minimizing off-target effects.

Acknowledgments

The contents of this publication do not represent the views of the Department of Veterans Affairs or the United States Government. The authors would like to acknowledge the efforts of Dr Rafal Pacholczyk in the Georgia Cancer Center Immune Monitoring Shared Resource for his assistance with the Luminex assays, the Augusta University Electron Microscopy and Histology Core (RRID:SCR_026810) for assistance with histological specimen preparation, and the Augusta University Cell Imaging Core (RRID:SCR_026799) for assistance with specimen imaging.

Author contributions

Jennifer Dorn (Data curation, Formal analysis, Investigation, Writing—original draft, Writing—review & editing), Dima W. Alhamad (Data curation, Formal analysis, Investigation, Methodology, Writing—review & editing), Husam Bensreti (Data curation, Formal analysis, Investigation, Methodology, Writing—review & editing), Christopher L. Yearwood (Investigation, Methodology, Writing—review & editing), Tate J. Allen (Investigation, Methodology, Writing—review & editing), Michaela Cushing (Data curation, Investigation, Methodology, Writing—review & editing), Joseph C. Shaver (Data curation,

Formal analysis, Investigation, Methodology, Writing—review & editing), Colby Gross (Investigation, Methodology, Writing—review & editing), William C. Whichard (Investigation, Methodology, Writing—review & editing), Caihong Dai (Investigation, Methodology, Writing—review & editing), Kanglun Yu (Investigation, Methodology, Project administration, Supervision, Writing—review & editing), Roger Zhong (Data curation, Formal analysis, Investigation, Methodology, Writing—review & editing), Marion A. Cooley (Funding acquisition, Investigation, Methodology, Writing—review & editing), Maribeth H. Johnson (Formal analysis. Investigation, Methodology, Writing—review & editing), Wendy B. Bollag (Investigation, Methodology, Writing—review & editing), Sadanand Fulzele (Investigation, Methodology, Writing—review & editing), Carlos M. Isales (Funding acquisition, Investigation, Methodology, Project administration, Writing—review & editing), Mark W. Hamrick (Funding acquisition, Investigation, Methodology, Writing—review & editing), William D. Hill (Conceptualization, Investigation, Methodology, Project administration, Writing—review & editing), and Meghan E. McGee-Lawrence (Conceptualization, Data curation, Formal analysis, Funding acquisition, Investigation, Methodology, Project administration, Resources, Supervision, Validation, Visualization, Writing—original draft, Writing—review & editing)

Supplementary material

Supplementary material is available at *JBMR Plus* online.

Funding

This study was supported by the National Institutes of Health (NIA P01 AG036675 Project 4, R01 AG 067510, S10 OD 025177). W.B.B. is supported by a Department of Veterans Affairs (VA) Career Scientist Award (IK6 BX00569).

Conflicts of interest

The authors state that they have no conflicts of interest.

Data availability

The data that support the findings of this study are available from the corresponding author upon reasonable request.

References

1. Ding KH, Cain M, Davis M, et al. Amino acids as signaling molecules modulating bone turnover. *Bone*. 2018 Oct;115:15–24. https://doi.org/10.1016/j.bone.2018.02.028
2. El Refaey M, Zhong Q, Hill WD, et al. Aromatic amino acid activation of signaling pathways in bone marrow mesenchymal stem cells depends on oxygen tension. *PLoS One*. 2014 Apr 11;9(4):e91108. https://doi.org/10.1371/journal.pone.0091108
3. El Refaey M, Watkins CP, Kennedy EJ, et al. Oxidation of the aromatic amino acids tryptophan and tyrosine disrupts their anabolic effects on bone marrow mesenchymal stem cells. *Mol Cell Endocrinol*. 2015 Jul 15;410:87–96. https://doi.org/10.1016/j.mce.2015.01.034
4. Kaiser H, Yu K, Pandya C, et al. Kynurenine, a tryptophan metabolite that increases with age, induces muscle atrophy and lipid peroxidation. *Oxid Med Cell Longev*. 2019 Oct 13;2019:9894238. https://doi.org/10.1155/2019/9894238
5. Wang Q, Liu D, Song P, Zou MH. Tryptophan-kynurenine pathway is dysregulated in inflammation, and immune activation. *Front Biosci (Landmark Ed)*. 2015;20(7):1116–1143.
6. Refaey ME, McGee-Lawrence ME, Fulzele S, et al. Kynurenine, a tryptophan metabolite that accumulates with age, induces bone loss. *J Bone Miner Res*. 2017 Nov;32:2182–2193. https://doi.org/10.1002/jbmr.3224
7. Elmansi AM, Hussein KA, Herrero SM, et al. Age-related increase of kynurenine enhances miR29b-1-5p to decrease both CXCL12 signaling and the epigenetic enzyme Hdac3 in bone marrow stromal cells. *Bone Rep*. 2020 Apr 23;12:100270. https://doi.org/10.1016/j.bonr.2020.100270
8. Sipahi H, Girgin G, Inanici F, Ariogul S, Sahin G, Baydar T. Tryptophan degradation and neopterin levels by aging. *Pteridines* 2013;24(1):33–39. https://doi.org/10.1515/pterid-2013-0008
9. Kim BJ, Hamrick MW, Yoo HJ, et al. The detrimental effects of kynurenine, a tryptophan metabolite, on human bone metabolism. *J Clin Endocrinol Metab*. 2019;104(6):2334–2342. https://doi.org/10.1210/jc.2018-02481
10. Eisa NH, Reddy SV, Elmansi AM, et al. Kynurenine promotes RANKL-induced osteoclastogenesis in vitro by activating the aryl hydrocarbon receptor pathway. *Int J Mol Sci*. 2020 Oct 26;21(21). https://doi.org/10.3390/ijms21217931
11. Kondrikov D, Elmansi A, Bragg RT, et al. Kynurenine inhibits autophagy and promotes senescence in aged bone marrow mesenchymal stem cells through the aryl hydrocarbon receptor pathway. *Exp Gerontol*. 2020 Feb;130:110805. https://doi.org/10.1016/j.exger.2019.110805
12. Dalton S, Smith K, Singh K, et al. Accumulation of kynurenine elevates oxidative stress and alters microRNA profile in human bone marrow stromal cells. *Exp Gerontol*. 2020 Feb;130:110800. https://doi.org/10.1016/j.exger.2019.110800
13. Pierce JL, Roberts RL, Yu K, et al. Kynurenine suppresses osteoblastic cell energetics in vitro and osteoblast numbers in vivo. *Exp Gerontol*. 2020 Feb;130:110818. https://doi.org/10.1016/j.exger.2019.110818
14. Bensreti H, Yu K, Alhamad DW, et al. Orchiectomy sensitizes cortical bone in male mice to the harmful effects of kynurenine. *Bone*. 2023 Aug;173:116811. https://doi.org/10.1016/j.bone.2023.116811
15. Sinclair LV, Neyens D, Ramsay G, Taylor PM, Cantrell DA. Single cell analysis of kynurenine and system L amino acid transport in T cells. *Nat Commun*. 2018 May 17;9(1):1981. https://doi.org/10.1038/s41467-018-04366-7
16. Wang W, Zou W. Amino acids and their transporters in T cell immunity and cancer therapy. *Mol Cell*. 2020 Nov 5;80(3):384–395. https://doi.org/10.1016/j.molcel.2020.09.006
17. Fiore A, Zeitler L, Russier M, et al. Kynurenine importation by SLC7A11 propagates anti-ferroptotic signaling. *Mol Cell*. 2022;82(5):920–932 e927. https://doi.org/10.1016/j.molcel.2022.02.007
18. Opitz CA, Litzenburger UM, Sahm F, et al. An endogenous tumour-promoting ligand of the human aryl hydrocarbon receptor. *Nature*. 2011 Oct 5;478(7368):197–203. https://doi.org/10.1038/nature10491
19. Walczak K, Langner E, Makuch-Kocka A, et al. Effect of tryptophan-derived AhR ligands, kynurenine, kynurenic acid and FICZ, on proliferation, cell cycle regulation and cell death of melanoma cells—in vitro studies. *Int J Mol Sci*. 2020 Oct 26;21(21). https://doi.org/10.3390/ijms21217946
20. Wu PY, Chuang PY, Chang GD, et al. Novel endogenous ligands of aryl hydrocarbon receptor mediate neural development and differentiation of Neuroblastoma. *ACS Chem Neurosci*. 2019 Sept 18;10(9):4031–4042. https://doi.org/10.1021/acschemneuro.9b00273
21. Wajda A, Lapczuk-Romanska J, Paradowska-Gorycka A. Epigenetic regulations of AhR in the aspect of immunomodulation. *Int J Mol Sci*. 2020 Sept 3;21(17). https://doi.org/10.3390/ijms21176404
22. Larigot L, Juricek L, Dairou J, Coumoul X. AhR signaling pathways and regulatory functions. *Biochim Open*. 2018 Jun 11;7:1–9. https://doi.org/10.1016/j.biopen.2018.05.001
23. Trikha P, Lee DA. The role of AhR in transcriptional regulation of immune cell development and function. *Biochim Biophys Acta Rev Cancer*. 2020 Jan;1873(1):188335. https://doi.org/10.1016/j.bbcan.2019.188335

24. Alhamad DW, Bensreti H, Dorn J, Hill WD, Hamrick MW, McGee-Lawrence ME. Aryl hydrocarbon receptor (AhR)-mediated signaling as a critical regulator of skeletal cell biology. *J Mol Endocrinol*. 2022 Aug 22;69(3):R109–R124. https://doi.org/10.1530/JME-22-0076
25. Yoshikawa Y, Izawa T, Hamada Y, et al. Roles for B[a]P and FICZ in subchondral bone metabolism and experimental temporomandibular joint osteoarthritis via the AhR/Cyp1a1 signaling axis. *Sci Rep*. 2021 Jul 21;11(1):14927. https://doi.org/10.1038/s41598-021-94470-4
26. Huang J, Wang Y, Zhou Y. Beneficial roles of the AhR ligand FICZ on the regenerative potentials of BMSCs and primed cartilage templates. *RSC Adv*. 2022 Apr 13;12(18):11505–11516. https://doi.org/10.1039/d2ra00622g
27. Korkalainen M, Kallio E, Olkku A, et al. Dioxins interfere with differentiation of osteoblasts and osteoclasts. *Bone*. 2009 Jun;44(6):1134–1142. https://doi.org/10.1016/j.bone.2009.02.019
28. Watson ATD, Nordberg RC, Loboa EG, Kullman SW. Evidence for aryl hydrocarbon receptor-mediated inhibition of osteoblast differentiation in human mesenchymal stem cells. *Toxicol Sci*. 2019;167(1):145–156. https://doi.org/10.1093/toxsci/kfy225
29. Zhou Y, Jiang R, An L, et al. Benzo[a]pyrene impedes self-renewal and differentiation of mesenchymal stem cells and influences fracture healing. *Sci Total Environ*. 2017 Jun 1;587-588:305–315. https://doi.org/10.1016/j.scitotenv.2017.02.152
30. Voronov I, Heersche JN, Casper RF, Tenenbaum HC, Manolson MF. Inhibition of osteoclast differentiation by polycyclic aryl hydrocarbons is dependent on cell density and RANKL concentration. *Biochem Pharmacol*. 2005 Jul 15;70(2):300–307. https://doi.org/10.1016/j.bcp.2005.04.028
31. Jia Y, Tao Y, Lv C, Xia Y, Wei Z, Dai Y. Tetrandrine enhances the ubiquitination and degradation of Syk through an AhR-c-src-c-Cbl pathway and consequently inhibits osteoclastogenesis and bone destruction in arthritis. *Cell Death Dis*. 2019 Jan 15;10(2):38. https://doi.org/10.1038/s41419-018-1286-2
32. Iqbal J, Sun L, Cao J, et al. Smoke carcinogens cause bone loss through the aryl hydrocarbon receptor and induction of Cyp1 enzymes. *Proc Natl Acad Sci USA*. 2013 Jul 2;110(27):11115–11120. https://doi.org/10.1073/pnas.1220919110
33. Dong W, Hinton DE, Kullman SW. TCDD disrupts hypural skeletogenesis during medaka embryonic development. *Toxicol Sci*. 2012 Jan;125(1):91–104. https://doi.org/10.1093/toxsci/kfr284
34. Yang JH, Lee HG. 2,3,7,8-Tetrachlorodibenzo-p-dioxin induces apoptosis of articular chondrocytes in culture. *Chemosphere*. 2010 Apr;79(3):278–284. https://doi.org/10.1016/j.chemosphere.2010.01.040
35. Huang Y, Furuno M, Arakawa T, et al. A framework for identification of on- and off-target transcriptional responses to drug treatment. *Sci Rep*. 2019 Nov 26;9 (1):17603. https://doi.org/10.1038/s41598-019-54180-4
36. Pierce JL, Sharma AK, Roberts RL, et al. The glucocorticoid receptor in Osterix-expressing cells regulates bone mass, bone marrow adipose tissue, and systemic metabolism in female mice during aging. *J Bone Miner Res*. 2022 Feb;37(2):285–302. https://doi.org/10.1002/jbmr.4468
37. Walisser JA, Bunger MK, Glover E, Bradfield CA. Gestational exposure of Ahr and Arnt hypomorphs to dioxin rescues vascular development. *Proc Natl Acad Sci USA*. 2004 Nov 23;101(47):16677–16682. https://doi.org/10.1073/pnas.0404379101
38. Walisser JA, Glover E, Pande K, Liss AL, Bradfield CA. Aryl hydrocarbon receptor-dependent liver development and hepatotoxicity aremediated by different cell types. *Proc Natl Acad Sci USA*. 2005 Dec 6;102(49):6. https://doi.org/10.1073/pnas.0504757102
39. Davey RA, Clarke MV, Sastra S, et al. Decreased body weight in young Osterix-Cre transgenic mice results in delayed cortical bone expansion and accrual. *Transgenic Res*. 2012 Aug;21(4):885–893. https://doi.org/10.1007/s11248-011-9581-z
40. Davis JL, Pokhrel NK, Cox L, Rohatgi N, Faccio R, Veis DJ. Conditional loss of IKKalpha in Osterix+ cells has no effect on bone but leads to age-related loss of peripheral fat. *Sci Rep*. 2022 Mar 22;12(1):4915. https://doi.org/10.1038/s41598-022-08914-6
41. Chen J, Shi Y, Regan J, Karuppaiah K, Ornitz DM, Long F. Osx-Cre targets multiple cell types besides osteoblast lineage in postnatal mice. *PLoS One*. 2014;9(1):e85161. https://doi.org/10.1371/journal.pone.0085161
42. Wang L, Mishina Y, Liu F. Osterix-Cre transgene causes craniofacial bone development defect. *Calcif Tissue Int*. 2015 Feb;96(2):129–137. https://doi.org/10.1007/s00223-014-9945-5
43. Matthews J, Gustafsson JA. Estrogen receptor and aryl hydrocarbon receptor signaling pathways. *Nucl Recept Signal*. 2006 Jul 7;4:e016. https://doi.org/10.1621/nrs.04016
44. Miki Y, Hata S, Ono K, et al. Roles of aryl hydrocarbon receptor in aromatase-dependent cell proliferation in human osteoblasts. *Int J Mol Sci*. 2017 Oct 17;18(10):2159. https://doi.org/10.3390/ijms18102159
45. Jang IY, Park JH, Kim JH, et al. The association of circulating kynurenine, a tryptophan metabolite, with frailty in older adults. *Aging (Albany NY)*. 2020 Nov 13;12(21):22253–22265. https://doi.org/10.18632/aging.104179
46. Emch MJ, Wicik Z, Aspros KGM, et al. Estrogen-regulated miRs in bone enhance osteoblast differentiation and matrix mineralization. *Mol Ther Nucleic Acids*. 2023 June 3;33:28–41. https://doi.org/10.1016/j.omtn.2023.05.026

JBMR Plus, 2025, 9, ziaf067
https://doi.org/10.1093/jbmrpl/ziaf067
Research Article